Applied Surface Science 357 (2015) 413–416

Contents lists available at ScienceDirect

Applied Surface Science

journal homepage: www.elsevier.com/locate/apsusc

The effect of high-temperature oxygen annealing on field emission from ZnO nanowire arrays

Si Chen [a], Jiangtao Chen [b], Jianlin Liu [c], Jing Qi [a,*], Yuhua Wang [d,*]

[a] The Key Laboratory for Magnetism and Magnetic Materials of MOE, School of Physical Science and Technology, Lanzhou University, Lanzhou 730000, China
[b] State Key Laboratory of Solid Lubrication, Lanzhou Institute of Chemical Physics, Chinese Academy of Sciences, 18 Tianshui Mid. Road, Lanzhou 730000, China
[c] Quantum Structures Laboratory, Department of Electrical and Computer Engineering, University of California, Riverside, CA 92521, USA
[d] Department of Material Science, School of Physical Science and Technology, Lanzhou University, Lanzhou 730000, China

ARTICLE INFO

Article history:
Received 14 July 2015
Received in revised form 25 August 2015
Accepted 2 September 2015

Keywords:
ZnO
Nanowire arrays
Oxygen annealing
Field emission
Oxygen vacancy

ABSTRACT

We obtained well-aligned ZnO nanowire arrays by chemical vapor deposition. The XRD patterns show that the crystallinity is improved by O_2 annealing at 800 °C. The field emission (FE) properties of annealed ZnO nanowire arrays become worse. The photoluminescence spectra show that the decrease of oxygen vacancy densities in ZnO nanowire arrays is responsible for the degraded FE properties.

1. Introduction

Zinc oxide, a wide band gap (3.37 eV) semiconducting, piezoelectric, and photoconducting material, has attracted a great deal of attention in recent years [1–3]. Its strong exciton binding energy of 60 meV makes it very attractive for exciton-based lasing applications. ZnO esp. its nanostructures, also has great potential in applications in optoelectronic devices [4], field effect transistors [5], waveguides [6], photocatalysis [7], sensors [8], surface acoustic solar cells [9], transparent conducting oxide nanocrystal inks [10], and field emitters [11].

Field emission (FE) properties of ZnO nanowire arrays have been widely studied [12–14]. Previous studies of FE from ZnO nanowires report performances such as turn-on field and emission-current stability. Few of them elucidate the underlying physics of FE. The FE properties could have some relationship with the resistance and the carrier density of ZnO nanowire arrays [15]. The resistance and carrier density of ZnO nanowire arrays are related to oxygen vacancy density, which can be changed by O_2 annealing, depending on annealing temperature and oxygen concentrations [16,17]. Meanwhile, the change of oxygen vacancy density can be detected by photoluminescence (PL) spectra, in which broad band of green emission is usually attributed to oxygen vacancy [16,18]. However, only a few studies reported the effects of O_2 annealing on the FE properties of ZnO nanostructures [19–21]. In these reports, the impact of O_2 annealing on the FE properties of ZnO nanostructures at low temperature and in different oxygen concentrations has been studied. However, changes of vacancy types and densities induced by annealing in oxygen at low temperature are different from that at high temperature [17]. At the same time, the impact of high-temperature O_2 annealing remains debatable.

In this paper, we report FE from ZnO nanowire arrays synthesized by chemical vapor deposition and significant changes of FE properties by O_2 post-annealing at high temperature. PL analysis shows the correlations between the degraded FE properties and oxygen vacancy densities in annealed ZnO nanowire arrays.

2. Experimental details

2.1. Synthesis of ZnO nanowire arrays

ZnO nanowire arrays were synthesized by chemical vapor deposition on ZnO seed layers. ZnO seed layers were grown on pre-cleaned [22] p^+-Si (100) substrates in a radio frequency plasma-assisted SVTA molecular beam epitaxy system. Zn source was provided by a regular Knudsen-cell filled with elemental Zn

* Corresponding authors.
E-mail addresses: qijing@lzu.edu.cn (J. Qi), wyh@lzu.edu.cn (Y. Wang).

http://dx.doi.org/10.1016/j.apsusc.2015.09.030
0169-4332/

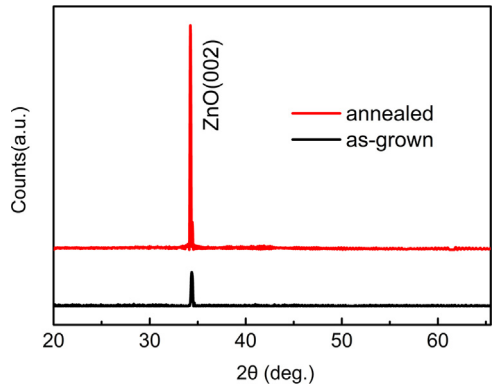

Fig. 1. XRD patterns of the as-grown and oxygen-annealed samples.

(6N). O source was provided by a radio frequency plasma source sustained with O_2 (6N) gas. A mass flow controller was used to precisely tune the O_2 flow rate. The ZnO layers were grown at 550 °C, with 345 °C Zn cell temperature, 5.0 sccm (standard cubic centimeter per minute) O_2 gas flow rate, and 400 W oxygen plasma power. The thickness of the seed layers is around 140 nm. Then the sample was transferred to a CVD quartz tube furnace. Analytical grade zinc powder (purity 99.99%) was employed as Zn source. The source material was placed in a quartz boat located in the center of the tube. The substrates were placed downstream of the carrier gas flow. The quartz tube was purged with 1000 sccm of argon and 1.5 sccm of oxygen during the whole nanowire arrays growth procedure. The pumping speed of a mechanical pump was regulated to maintain the pressure inside the quartz tube at the lowest level during the evaporation. Then the furnace temperature was raised to 700 °C at a rate of 10 °C/min. After growth for 30 min, the furnace was cooled naturally down to room temperature.

2.2. Annealing processing of the obtained nanoarrays

The annealing procedure had been performed under ambient pressure at a temperature of 800 °C for 60 min with a constant oxygen flow of 50 sccm. After annealing, the furnace was cooled naturally down to room temperature.

2.3. Characterizations and measurements of the obtained nanoarrays

The crystal structure and chemical nature of as-grown and oxygen-annealed ZnO nanowire arrays were analyzed using X-Ray diffractometry (XRD, D2 Phaser, bruker) with Cu K radiation (=1.54184 Å) operating at 30 kV and 10 mA. The morphology of the samples was obtained utilizing a scanning electron microscope (SEM, S3400N, Hitachi). The FE properties were measured at a pressure of 6×10^{-6} Pa. The PL spectra were measured by a Fluorlog-3 spectrofluorometer equipped with Xe900 (450 W xenon arc lamp, Horiba Jobin Yvon) as the excitation source utilizing an excitation wavelength of 325 nm. The emission spectra were measured by a monochromator (TM300) while the resolution of the grating is 0.05 nm with standard 1800 g/mm.

3. Results and discussion

3.1. Crystallinity and surface morphology

The XRD patterns of as-grown and oxygen-annealed samples are shown in Fig. 1. The degree of the orientation can be illustrated by the relative texture coefficient [23], which is given by

$$TC_{002} = \frac{I_{002}/I^0_{002}}{(I_{002}/I^0_{002}) + (I_{102}/I^0_{102})}$$

In the equation, TC_{002} is the relative texture coefficient of diffraction peaks (002) over (102), I_{002} and I_{102} are the measured diffraction intensities due to (002) and (102) planes, respectively, $I^0{}_{002}$ and $I^0{}_{102}$ are the corresponding values of standard PDF measured from randomly oriented powder samples. For materials with random crystallographic orientations, e.g. powders, the texture coefficient is 0.5. The values of both samples are 1, which indicates an extremely high c-orientation of the samples. The lattice constants of the as-grown and oxygen-annealed samples are measured to be c = 5.209 Å, and 5.225 Å, respectively, which are consistent with the standard values (JCPDS: 80-0074, c = 5.215 Å). The values of full width at half maximum (FWHM) are 0.149° and 0.073° for the as-grown and oxygen-annealed samples, respectively. The XRD results reveal that the synthesized ZnO nanowire arrays have well crystalline hexagonal-wurtzite structure, and crystallinity of ZnO nanowire arrays is improved by O_2 annealing.

Fig. 2(a) and (b) shows typical top-view and side-view SEM surface morphology of the as-grown sample. As can be seen, aligned nanowire arrays are evident. The average diameter and length of the nanowires are about 90 nm and 4.5 μm, respectively. The inset in Fig. 1(a) shows further magnified image of one nanowire, which indicates that the nanowire arrays are c-oriented. The result is in accordance with that of XRD. O_2 annealing did not change the surface morphology, which is not shown here.

3.2. FE properties

Fig. 3 shows emission current density as a function of the applied electric field (J–E) of the as-grown and annealed samples, respectively. Here we define the turn-on field (E_{t0}) as an electric field to produce a current of 0.1 mA/cm^2. The FE results show that the values of E_{t0} are estimated to be 5.32 V/μm and 6.56 V/μm for the as-grown and annealed samples, respectively. The low E_{t0} could originate from the good alignment of the nanowire arrays. E_{t0} becomes larger after the sample is annealed in oxygen. In other

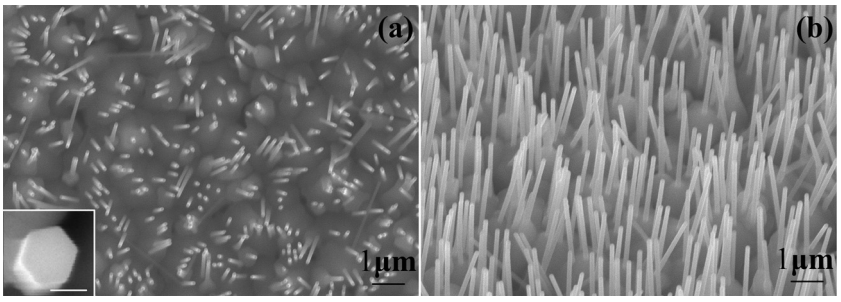

Fig. 2. SEM images of the as-grown sample: (a) top view, (b) side view. The inset shows further magnified image of one nanowire, the scale bar is 50 nm.

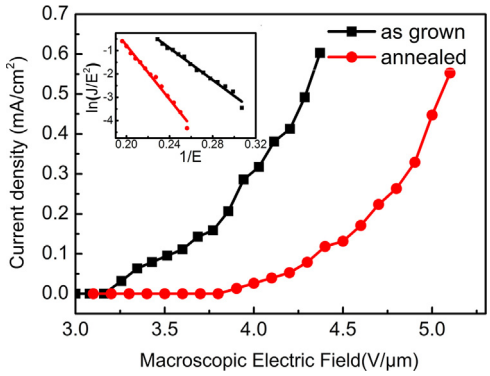

Fig. 3. J–E plot of FE from the ZnO nanowire arrays. The inset shows the corresponding FN plot.

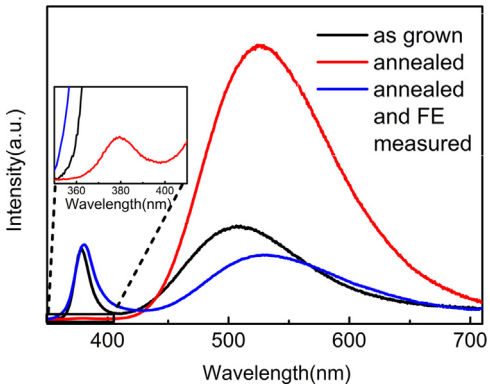

Fig. 4. PL spectra of the as-grown, oxygen-annealed, and oxygen-annealed-and-FE-measured samples. The inset shows the PL spectra of the oxygen-annealed sample in the region of 350–410 nm.

words, the FE properties degrade due to the O_2 annealing. We measured the FE properties of the annealed sample for several times, only tiny changes were observed. In the inset of Fig. 3, the Fowler-Nordheim (FN) plots show a roughly linear relationship for both samples, implying that a quantum tunneling mechanism is responsible for the emission [19]. For the FN emission,

$$J = \left(\frac{A\beta^2E^2}{\varphi}\right)\exp\left(\frac{-B\varphi^{3/2}}{\beta E}\right)$$

where J is the current density, E is the applied field strength, φ is work function of the emitter material (5.3 eV for as-grown ZnO [20]), A and B are constant with the value of 1.56×10^{-10} (AV^{-2} eV) and 6.83×10^3 ($VeV^{-3/2}$ μm^{-1}), respectively, and β is the field enhancement factor which is associated with the magnitude of electric field at the emitting surface by $E_{local} = \beta E$, E_{local} is the local electric field at the emitting surface. Based on the slope of the plot of $\ln(J/E^2)$ versus $1/E$ in the inset of Fig. 3, β was estimated to be approximately 2746 for as-grown sample, which is high enough for various FE applications. The field enhancement factor β is highly dependent on the geometrical morphology and alignment of the nanowire arrays [24,25], and such a high-field enhancement factor could be attributed to the good alignment of the ZnO nanowire arrays as well. Since the morphology and alignment of the ZnO nanowire arrays are not changed after annealing, we reasonably assume that the β values of the two samples are the same. Therefore, the variation in the slope $k = -B\varphi^{3/2}d/\beta$ of FN plots reflects the change in the work function φ of ZnO nanowire arrays since d remains unchanged. According to the FN plots in the inset of Fig. 3, and taking the work function φ of the as-grown ZnO nanowire as 5.3 eV [19], the work function φ is estimated to be 7.29 eV for the oxygen-annealed sample. Compared with as-grown sample, the work function is increased by 1.99 eV through O_2 annealing.

3.3. PL properties

According to previous reports, the degraded FE properties could result from the increase of the resistivity, decrease of carrier densities and band bending of ZnO nanowire arrays [15,26]. Both decrease of carrier densities and band bending of ZnO nanowire arrays could increase the work function [26,27]. Annealing the ZnO nanowire arrays in oxygen at high temperature can lead to higher resistivity because the oxygen vacancy density decreases. The annealing can also lead to upward band bending because chemisorption of oxygen at the ZnO surface caused by high-temperature O_2 annealing. The chemisorbed oxygen at the ZnO surface can capture electrons in a region near the surface, and as a consequence, nonradiative recombination between photogenerated electrons and holes will occur and the NBE emissions will be suppressed [18]. Fig. 4 shows PL spectra of as-grown sample, oxygen-annealed sample, and sample that has undergone both annealing and FE measurement, respectively. All samples exhibit both near band edge (NBE) emission and green emission peaks. The green peak of the annealed sample increases and the NBE peak decreases greatly, which originates from the chemisorption of the oxygen ions [18,28]. After the annealed sample went through FE measurement, the green peak reduces and the NBE peak increases to the level before O_2 annealing. In other words, desorption of oxygen ions occurred during FE measurement. As a result, band bending also reduces greatly during FE measurement. Considering that FE properties were not significantly changed after the first FE measurement, band bending is not main reason for the degraded FE properties. Compared to the as-grown sample, the green peak of the sample going through both annealing and FE measurement is weaker. The result means lower oxygen vacancy density compared to the as-grown sample, in other words, higher quality of the nanowire arrays, which is consistent with the XRD results shown in Fig. 1. So, it can be concluded that the degrading of FE properties are mainly due to the lower carrier densities and higher resistivity caused by less oxygen vacancies rather than adsorption of negative charged oxygen ion on the surface.

4. Conclusion

In summary, we obtained well-aligned ZnO nanowire arrays by chemical vapor deposition. The O_2 annealing at high temperature degrades FE properties of ZnO nanowire arrays. The PL spectra show that the ratio between deep level green and NBE emissions are significantly changed for the samples before and after annealing in oxygen. The degraded FE properties are mainly caused by the decrease of oxygen vacancy density during high temperature O_2 annealing.

Acknowledgements

This work was supported by National Natural Science Foundation of China (nos. 50902065, 11474137, 51402139), Open Project of Key Laboratory for Magnetism and Magnetic Materials of the Ministry of Education, Lanzhou University (LZUMMM2015012), National Nature Science Young Foundation of China (no. 10904057).

References

[1] R. Chen, Q. Ye, T. He, T. Van Duong, Y. Ying, Y.Y. Tay, T. Wu, H. Sun, Exciton localization and optical properties improvement in nanocrystal-embedded ZnO core–shell nanowires, Nano Lett. 13 (2013) 734–739.

[2] S. Kulinich, T. Kondo, Y. Shimizu, T. Ito, Pressure effect on ZnO nanoparticles prepared via laser ablation in water, J. Appl. Phys. 113 (2013), 033509-033509-5.
[3] J. Song, S. Kulinich, J. Yan, Z. Li, J. He, C. Kan, H. Zeng, Epitaxial ZnO nanowire-on-nanoplate structures as efficient and transferable field emitters, Adv. Mater. 25 (2013) 5750–5755.
[4] S. Chu, G. Wang, W. Zhou, Y. Lin, L. Chernyak, J. Zhao, J. Kong, L. Li, J. Ren, J. Liu, Electrically pumped waveguide lasing from ZnO nanowires, Nat. Nanotechnol. 6 (2011) 506–510.
[5] H. Ng, J. Han, T. Yamada, P. Nguyen, Y. Chen, M. Meyyappan, Crystal nanowire vertical surround-gate field-effect transistor, Nano Lett. 4 (2004) 1247–1252.
[6] C. Gorla, N. Emanetoglu, S. Liang, W. Mayo, Y. Lu, M. Wraback, H. Shen, Structural, optical, and surface acoustic wave properties of epitaxial ZnO films grown on ($01\bar{1}2$) sapphire by metalorganic chemical vapor deposition, J. Appl. Phys. 85 (1999) 2595–2602.
[7] B. Wang, L. Zong, R. Lv, Y. Sun, Y. Zhu, Performance enhancement of ZnO photocatalyst via synergic effect of surface oxygen defect and graphene hybridization, Langmuir 29 (2013) 3097–3105.
[8] D. Gedamu, I. Paulowicz, S. Kaps, O. Lupan, S. Wille, G. Haidarschin, Y. Mishra, R. Adelung, Rapid fabrication technique for interpenetrated ZnO nanotetrapod networks for fast UV sensors, Adv. Mater. 26 (2014) 1541–1550.
[9] S. Ko, D. Lee, H. Kang, K. Nam, J. Yeo, S. Hong, C. Grigoropoulos, H. Sung, Nanoforest of hydrothermally grown hierarchical ZnO nanowires for a high efficiency dye-sensitized solar cell, Nano Lett. 11 (2011) 666–671.
[10] J. Song, S. Kulinich, J. Li, Y. Liu, H. Zeng, A general one-pot strategy for the synthesis of high-performance transparent-conducting-oxide nanocrystal inks for all-solution-processed devices, Angew. Chem. Int. Ed. 54 (2015) 462–466.
[11] S. Garry, É. McCarthy, J. Mosnier, E. McGlynn, Influence of ZnO nanowire array morphology on field emission characteristics, Nanotechnology 25 (2014) 407–412.
[12] Y. Zhang, C. Lee, Site-controlled growth and field emission properties of ZnO nanorod arrays, Appl. Surf. Sci. 259 (2012) 562–565.
[13] C. Lee, T. Lee, S. Lyu, Y. Zhang, Field emission from well-aligned zinc oxide nanowires grown at low temperature, Appl. Phys. Lett. 81 (2002) 3648–3650.
[14] Y. Liu, C. Li, J. Wang, X. Fan, G. Yuan, S. Xu, M. Xu, J. Zhang, Y. Zhao, Field emission properties of ZnO nanorod arrays by few seed layers assisted growth, Appl. Surf. Sci. 331 (2015) 497–503.
[15] J. You, X. Zhang, P. Cai, J. Dong, Y. Gao, Z. Yin, N. Chen, R. Wang, H. Yan, Enhancement of field emission of the ZnO film by the reduced work function and the increased conductivity via hydrogen plasma treatment, Appl. Phys. Lett. 94 (2009), 262105-1-262105-3.
[16] K. Vanheusden, C. Seager, W. Warren, D. Tallant, J. Voigt, Correlation between photoluminescence and oxygen vacancies in ZnO phosphors, Appl. Phys. Lett. 68 (1996) 403–405.
[17] H. Zeng, G. Duan, Y. Li, S. Yang, X. Xu, W. Cai, Blue luminescence of ZnO nanoparticles based on non-equilibrium processes: defect origins and emission controls, Adv. Funct. Mater. 20 (2010) 561–572.
[18] D. Wang, H. Seo, C. Tin, M. Bozack, J. Williams, M. Park, N. Sathitsuksanoh, A. Cheng, Y. Tzeng, Effects of postgrowth annealing treatment on the photoluminescence of zinc oxide nanorods, J. Appl. Phys. 99 (2006) 113509–113513.
[19] Q. Zhao, X. Xu, X. Song, X. Zhang, D. Yu, Enhanced field emission from ZnO nanorods via thermal annealing in oxygen, Appl. Phys. Lett. 88 (2006), 033102-1-033102-3.
[20] K. Park, Y. Choi, M. Ahn, D. Kim, Y. Sung, J. Park, K. Choi, Enhancement of field-emission properties in ZnO nanowire array by post-annealing in H_2 ambient, J. Nanosci. Nanotechnol. 9 (2009) 4328–4332.
[21] W. Bai, X. Zhu, Z. Zhu, J. Chu, Synthesis of zinc oxide nanosheet thin films and their improved field emission and photoluminescence properties by annealing processing, Appl. Surf. Sci. 254 (2008) 6483–6488.
[22] J. Qi, J. Ren, M. Olmedo, N. Zhan, J. Liu, Unipolar resistive switching in Au/Cr/$Mg_{0.84}Zn_{0.16}O_{2-\delta}$/$p^+$-Si, Appl. Phys. A 107 (2012) 891–897.
[23] Y. Kajikawa, S. Noda, H. Komiyama, A simple index to restrain abnormal protrusions in films fabricated using CVD under diffusion-limited conditions, Chem. Vap. Deposition 10 (2004) 221–228.
[24] Q. Zhao, H. Zhang, Y. Zhu, S. Feng, X. Sun, J. Xu, D. Yu, Morphological effects on the field emission of ZnO nanorod arrays, Appl. Phys. Lett. 86 (2005) 203115–203121.
[25] X. Wang, J. Zhou, C. Lao, J. Song, N. Xu, Z. Wang, In situ field emission of density-controlled ZnO nanowire arrays, Adv. Mater. 19 (2007) 1627–1631.
[26] C. Zhao, K. Huang, S. Deng, N. Xu, J. Chen, Investigation of the effects of atomic oxygen exposure on the electrical and field emission properties of ZnO nanowires, Appl. Surf. Sci. 270 (2013) 82–89.
[27] H. Kang, J. Kang, S. Pang, E. Shim, S. Lee, Variation of light emitting properties of ZnO thin films depending on post-annealing temperature, Mater. Sci. Eng. B102 (2003) 313–316.
[28] Y. Lao, D. Wang, J. Huang, D. Steeves, B. Kimball, Z. Ren, Synthesis and photoluminescence studies on ZnO nanowires, Nanotechnology 15 (2004) 404–409.